Time-Resolved Detection of Transient Movement of Helices F and G in Doubly Spin-Labeled Bacteriorhodopsin

Nicole Radzwill, Klaus Gerwert, and Heinz-Jürgen Steinhoff
Lehrstuhl für Biophysik, Ruhr-Universität Bochum, D-44780 Bochum, Germany

ABSTRACT Photo-excited structural changes of the light-driven proton pump bacteriorhodopsin were monitored using double-site-directed spin labeling combined with electron paramagnetic resonance (EPR) spectroscopy. The inter-spin distances between nitroxides attached at residue positions 100 and 226, 101 and 160, and 101 and 168 were determined for the BR initial state and the trapped M photo-intermediate. Distance changes that occur during the photocycle were followed with millisecond time resolution under physiological conditions at 293 K. The kinetic analysis of the EPR data and comparison with the absorbance changes in the visible spectrum reveal an outward movement of helix F during the late M intermediate and a subsequent approach of helix G toward the proton channel. The displacements of the cytoplasmic moieties of these helices amount to 0.1–0.2 nm. We propose that the resulting opening of the proton channel decreases the pK of the proton donor D96 and facilitates proton transfer to the Schiff base during the M-to-N transition.

INTRODUCTION

The integral membrane protein bacteriorhodopsin (BR) acts as a light-driven proton pump in the purple membrane of *Halobacterium salinarum*. Its seven transmembrane helices bury the chromophore retinal that is bound via a protonated Schiff base to K216. Absorption of a photon initiates the all-*trans* to 13-*cis* photoisomerization of the retinal and triggers a catalytic cycle, the so-called photocycle, which results in an unidirectional transport of a proton from the cytoplasm to the extracellular surface (for reviews see Lanyi, 1998; Haupts et al., 1999).

A widely accepted model describes the photocycle as the sequential formation and decay of the optically characterized intermediates J, K, L, M, N, and O (Váró and Lanyi, 1991; Hessling et al., 1993). On the molecular level the cycle consists of a sequence of steps of isomerization, proton transport, and accessibility changes of the amino acids that can be either protonated or deprotonated. There is evidence that the retinal isomerization gives rise to structural changes as a key event for retinal protein function in general. The extent of the conformational change of bacteriorhodopsin is still under debate. It varies, depending on the experimental methods, from rearrangements of amino acid side chains to global helix movements (Vonck, 1996; Hessling et al., 1997; Thorgeirsson et al., 1997; Oka et al., 1999; Subramaniam et al., 1999; Vonck, 2000; Subramaniam and Henderson, 2000; Xiao et al., 2000). Diffraction studies suggest changes at helices B, C, F, and G. The major changes in the region of helices F and G were found to occur later in time than the changes near B and C (Dencher et al., 1989; Subramaniam et al., 1993; Kamikubo et al., 1996). A widening of the proton channel by an outward movement of helix F has been postulated for wild-type bacteriorhodopsin (Subramaniam et al., 1999) and for different mutants (Vonck, 1996; Rink et al., 2000). Electron diffraction of a triple mutant presumed to stabilize the full extent of the conformational change even in the initial state indicates an outward tilt of helix F and a displacement of helix G into the direction of helix F (Subramaniam and Henderson, 2000). X-ray data of the M intermediate of the wild type support an outward tilt of helix F in the region from V167 to V179, accompanied by a narrowing of the helical turn in helix G from residue L221 to R227 (Sass et al., 2000). However, no information about the conformational changes of the loop regions is available on the atomic level due to high disorder and the subsequent high-temperature factors (Luecke et al., 1999).

The timing of the conformational changes and the arrangement within the photocycle is also discussed controversially. Structural changes are found in M and in N, with the Schiff base protonated or deprotonated, respectively. One reason is due to the different stabilization methods used to trap the intermediate of interest to make them accessible for methods with low time resolution. However, in many cases not only M, but a mixture of L, M, and N is stabilized because significant back reactions between these intermediates take place (Hessling et al., 1993). This renders the assignment of the conformational change to M or N difficult. In addition, two M intermediates were shown to exist (Zimanyi et al., 1992; Druckmann et al., 1992; Hessling et al., 1993) with the deprotonated Schiff base either oriented toward the proton release side (M_1) or toward the proton uptake side (M_2). This reorientation of the Schiff base determines the vectoriality of the proton pump. Results of time-resolved electron paramagnetic resonance (EPR) spectroscopy provide also strong evidence for the existence of two different M intermediates. Kinetic analysis of a series of spin-labeled mutants provides evidence that a movement of

Received for publication 27 October 2000 and in final form 15 March 2001.

Address reprint requests to Dr. H.-J. Steinhoff, Max-Planck-Institute for Molecular Physiology, Otto-Hahn-Strasse 11, D-44227 Dortmund, Germany. Tel.: 49-234-322-4463; Fax: 49-234-321-4626; E-mail: hjs@bph.ruhr-uni-bochum.de.

0006-3495/01/06/2856/11 $2.00

helix F occurs during the M_1-to-M_2 transition, and subsequently, a rearrangement of side-chain orientations in the vicinity of the proton donor D96 takes place (Steinhoff et al., 1994; Rink et al., 2000; Mollaaghababa et al., 2000).

In the present approach we apply time-resolved EPR spectroscopy in combination with site-directed spin labeling (SDSL), which is a sensitive tool to define elements of secondary structure, including their solvent exposure, to characterize protein topography and to determine orientations and movements of individual segments of membrane proteins under physiological conditions (for reviews see Hubbell et al., 1996, 1998; Feix and Klug, 1998). The simultaneous exchange of two native amino acids by cysteines followed by modification with methane thiosulfonate spin labels provides a powerful way to estimate inter-residual distances under conditions relevant to function (for a review see Hustedt and Beth, 1999). This method has been successfully applied to a series of protein mutants in solution and in the crystal, e.g., rhodopsin (Farrens et al., 1996), insulin (Steinhoff et al., 1997), lysozyme (Mchaourab et al., 1997), bacteriorhodopsin (Thorgeirsson et al., 1997), Tet repressor (Tiebel et al., 1999), a potassium channel (Perozo et al., 1999), or reverse transcriptase (Kensch et al., 2000). By means of double-site-directed spin labeling (DSDSL) we determine distances and follow distance changes between the cytoplasmic ends of helix C and helices F and G, respectively. The assignment of the conformational changes to the respective intermediates was controlled by Fourier transform infrared (FT-IR) and visible (VIS) spectroscopy.

MATERIALS AND METHODS

Mutagenesis and mutant expression

The site-specific mutants of bacteriorhodopsin were prepared according to Ferrando et al. (1993) by means of the shuttle plasmid pEF191 using the *Bam*HI-*Hind*III restriction fragment, which encodes the entire *bob* gene. Mutagenesis was followed by transformation and homologous expression in *Halobacterium salinarum* strain MPK40 (Krebs et al., 1991; Rammelsberg et al., 1998). Mutated proteins were isolated as purple membrane sheets according to Oesterhelt and Stoeckenius (1974). The mutations were confirmed from *H. salinarum* transformants by DNA sequencing of the *bob* gene.

Spin labeling

Before spin labeling, the protein was incubated with 10 mM dithiothreitol (DTT) or 10 mM β-mercaptoethanol (β-Me) for several hours. Directly after removing the reductants by centrifugation, a 10:1 spin label (1-oxyl-2,2,5,5-tetramethylpyroline-3-methyl-sulfonate, R1) to protein concentration ratio was adjusted. Therefore, 50 μl of a 50 mM spin label stock solution in DMSO was added to 1 ml of suspension of membranes in 0.1 M phosphate buffer (pH 6.8), 0.1 M NaCl. The solution was incubated for 12 h at 20°C. The unbound spin label was then removed by multiple washing steps and subsequent resuspension, and 10–50 μl of the purple membrane suspension was used for EPR measurements at a final protein concentration of between 250 and 500 μM. The ratio of bound spin label to bacteriorhodopsin was determined for each mutant by double integration of the EPR spectrum and optical spectroscopy.

Treatment of L100C with β-Me or DTT before spin labeling leads to different label efficiencies: The ratio of bound spin label to protein was 0.3 for $^{\beta\text{-Me}}$L100R1 (treated with β-Me before spin labeling) and 0.8 for $^{\text{DTT}}$L100R1 (treated with DTT before spin labeling). The spectrum of $^{\text{DTT}}$L100R1 reveals three components that are due to different mobility of the nitroxide side chain R1 (see Fig. 4 *a*). The sharp lines represent unbound spin label (~15%). Peaks due to a mobile and an immobile component of the bound spin label are visible in the spectrum of $^{\text{DTT}}$L100R1. The mobile component is absent in the spectrum of $^{\beta\text{-Me}}$L100R1 (see also Rink et al., 2000). This may be due to an insufficient protection efficiency of our β-Me treatment against oxidation of the cysteine (Lamoureux and Whitesides, 1993) or an incomplete removal of β-Me from the exposed site. All further discussions are referred to the cysteine mutants prepared with DTT.

EPR continuous-wave-measurements and inter-spin distance determination

EPR spectra were recorded as previously described (Steinhoff et al., 1997; Pfeiffer et al., 1999). The determination of the inter-spin distances from the low-temperature spectra (T = 170 K) were performed by fitting simulated powder spectra to experimental data according to the method of Steinhoff et al. (1997). To distinguish the line broadening due to the dipolar interaction from the intrinsic line width, the magnetic and line width parameters in the absence of any spin-spin interaction were determined from the superposition of singly spin-labeled samples. The final values of the fitted g and A tensors are g_{xx} = 2.0083, g_{yy} = 2.0065, g_{zz} = 2.0028, A_{xx} = 5.2 G, A_{yy} = 3.5 G, and A_{zz} = 36.5 G. The calculated powder spectrum had to be convoluted with a field-independent line shape function, composed of a superposition of 31% Lorentzian and 69% Gaussian of 4.6 and 3.1 G width, respectively.

In addition, the distance between the spins was calculated from the dipole-dipole interaction component of the second moment of the absorption line, $\langle \Delta B_D^2 \rangle$ (Van Vleck, 1948; Abragam, 1961; Likhtenstein, 1976):

$$\langle \Delta B_D^2 \rangle = \frac{3}{5} g^2 \beta^2 S(S+1) \sum_j r_{ij}^{-6},$$

where g is the gyromagnetic ratio and β is the Bohr magneton. This parameter is unaffected by any scalar interaction among the spins; in particular, exchange interaction does not contribute. In the case of a radical pair, the correlation between the second moment and the distance is given by $r = 2.32 \times 10^8 / \langle \Delta B_D^2 \rangle^{1/6}$ nm, if $\langle \Delta B_D^2 \rangle$ is given in T^2. In practice, the dipole-dipole component of the second moment of an EPR line is calculated from the difference between the second moments for a pair of interacting spins and for a system without any interaction, i.e., the superposition of the spectra of the singly labeled protein samples.

Time-resolved EPR spectroscopy and flash photolysis

Light pulses generated by a xenon flash lamp at ~80-J electrical pulse energy and 30-μs pulse duration were used for photo-excitation. Difference spectra between the photo-activated state and the initial state were determined during a B-field scan by subtraction of the signals averaged within two different sampling intervals starting with different delays after the light flash. The length of the sampling intervals were set to 500 ms, and the delay times were set to 0 ms and 500 ms, respectively. Following this scheme, the spectrum recorded during the first time interval is a mixture of the photo-intermediates. The spectrum determined during the second sample interval represents the recovered initial state spectrum.

The EPR kinetics was followed at fixed B-field values where the difference spectrum showed a local extreme. The spectral changes were recorded with the integration time of the phase-sensitive detector set to 1

ms. Each transient consists of 16,000 data points sampled with a rate of 2000 s^{-1}. A total of 1000 transients were averaged before data analysis.

Absorbance changes in the visible spectral range were monitored by a conventional photolysis setup as described previously (Rammelsberg et al., 1997).

FT-IR spectroscopy

The BR−M steady-state spectra were recorded on a Bruker IFS66 FT-IR spectrometer equipped with an Oxford DN704 cryostat as described in detail in Hessling et al. (1997). The samples were light adapted at 285 K and subsequently cooled to 245 K, 235 K, or 220 K. The low-temperature spectra were measured with 2.0-cm^{-1} spectral resolution by averaging 50 interferograms before and after illumination of the samples with the light of a 100-W halogen lamp, which had passed through a Schott KG2 and OG 590 filter.

Molecular modeling and molecular dynamics simulations

Insight II software (Molecular Simulations, San Diego, CA) was used to model the spin-labeled BR with the data set [1BRR] (Brookhaven Data Bank) (Essen et al., 1998). Reorientation trajectories of the bound nitroxides were calculated from molecular dynamics (MD) simulations by means of the GROMOS program library (Biomos, Groningen, The Netherlands). After energy minimization, the system was equilibrated at 400 K and then heated up to 600 K. This temperature was chosen to guarantee the total space accessible for the reorientation of the nitroxides to be covered within reasonable computation time. Backbone atoms were restrained during the simulations. The MD simulations were performed for 6 ns with the time step of the integration of the equations of the motion set to 2 fs.

RESULTS

Spin-labeled sites

In the present approach the magnitude of helix displacements is derived from the inter-spin distance changes within pairs of nitroxide side chains. Because this approach may include significant contributions from nitroxide side-chain rearrangements in addition to the backbone movements, surface sites have been found to be the most suitable choice for measuring accurate distance changes (Hubbell et al., 2000). The bias due to a possible rearrangement of a single nitroxide side chain is further minimized by the choice of sites that show no or only minor mobility change during the BR photocycle. Consequently, we base our study on sites L100, A160, A168, and S226, which fulfill this requirement (Rink et al., 2000). A prominent mobility change is visible for the nitroxide side-chain V101R1 (Steinhoff et al., 1994). However, this mobility change seems not to be accompanied by a significant displacement of the nitroxide as will be shown later.

The positions of the spin labeled residues are shown in Fig. 1 according to the structural data of Essen et al. (1998). Residue L100 defines the end of helix C, and V101 is the first residue in the C-D loop. A160 represents the first residue of the E-F loop, A168 is located in the first α-helical turn of helix F, and S226 in the last α-helical turn of helix G. The doubly spin-labeled cysteine mutants L100R1&S226R1, V101R1&A160R1, and V101R1&A168R1 allow distance determinations between helices C and E, C and F, and C and G, respectively.

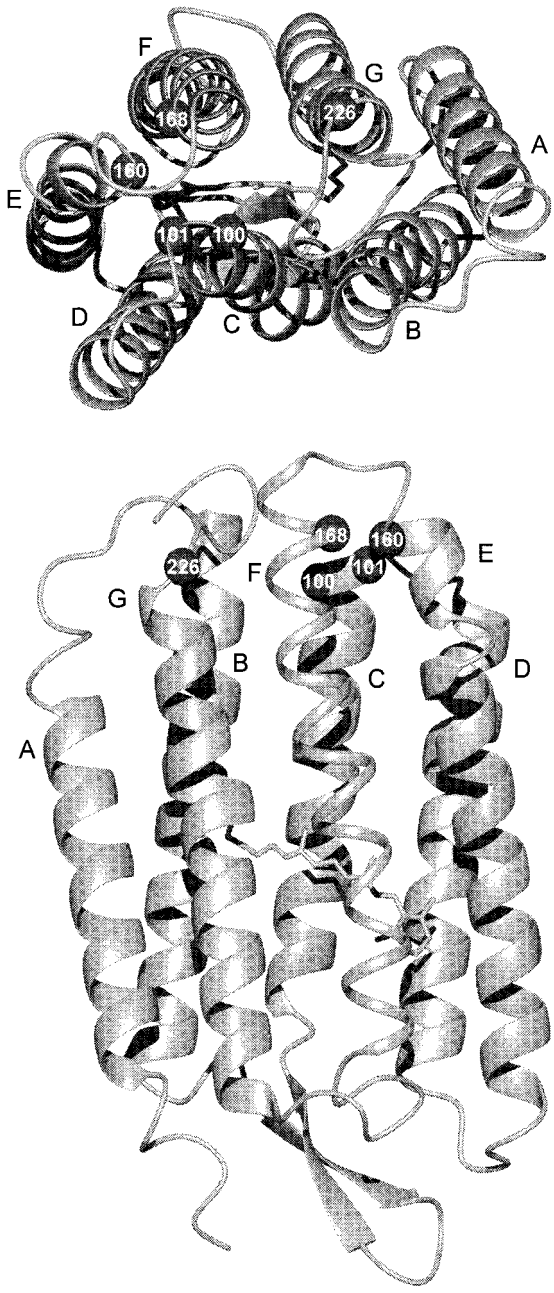

FIGURE 1 View onto the cytoplasmic side and side view of bacteriorhodopsin according to the data of Essen et al. (1998). The C_α atoms of those residues that were replaced by cysteines are shown as space-filled balls. The substituted amino acids were modified with the spin label MTSSL in pairs: L100C&S226C, V101C&A160C, and V101C&A168C.

Determination of inter-spin distances in the frozen state

All residue positions used in the doubly spin-labeled samples were first analyzed as single cysteine mutants. The BR

molecules are tightly packed in the purple membrane, and the possibility of spin-spin interactions between spin labels attached to different BR molecules has to be considered. To avoid possible averaging of the anisotropic dipolar interaction the dynamics of the spin label side chains and the rotational motion of bacteriorhodopsin was frozen ($T = 170$ K). However, the spectra of the single mutants L100R1, V101R1, A160R1, A168R1, and S226R1 did not show any evidence for considerable line broadening due to spin-spin interaction.

The BR initial-state spectra of the spin-labeled double mutants were recorded after light adaptation at room temperature and fast cooling to 170 K in the dark. To stabilize the M intermediate, bacteriorhodopsin was illuminated ($\lambda >$ 590 nm) at temperatures between 210 K and 250 K in steps of 10 K. After 10 min of illumination the sample was cooled to 170 K within approximately 1 min. The largest spectral changes compared with the BR initial state were found with samples illuminated in the temperature range between 220 K and 230 K.

To determine the composition of intermediates trapped by the described freezing procedure, FT-IR spectroscopy was performed. In the fingerprint region between 1330 cm^{-1} and 1100 cm^{-1} the difference spectrum initial state − photo-excited state of L100R1&S226R1 recorded at 220 K, 235 K, and 245 K shows typical features of the M intermediate (Fig. 2). The negative difference band at 1186 cm^{-1} is characteristic for a deprotonated Schiff base, the amplitude of which is known to be directly correlated to the amount of BR trapped in the M intermediate. The difference band at 1761 cm^{-1} reflects protonation of D85. Deprotonation of D85, as it would occur in the N intermediate, would shift this band to 1755 cm^{-1}. The amide I ratio (1670:1660 cm^{-1}) is <1 for 220 K and 235 K but exceeds 1 for 245 K, indicating a small admixture of an M_N intermediate or N at the higher temperature. We conclude from the features characteristic for the deprotonation of the Schiff base and the protonation of D85 that the intermediate trapped in the temperature range between 220 K and 230 K is identical to the M intermediate. At 245 K structural changes become visible in the amide I region.

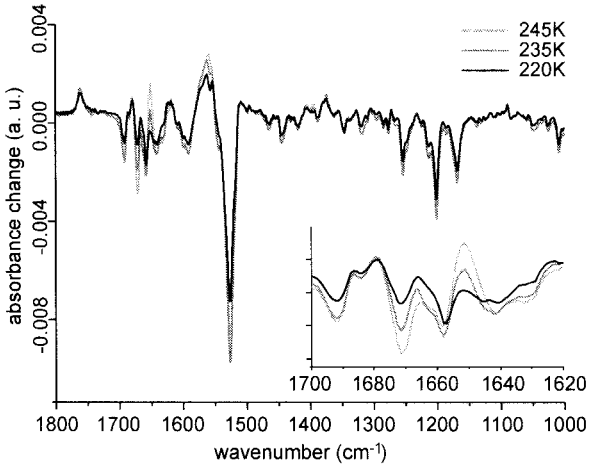

FIGURE 2 FT-IR difference spectra (initial state − photo-excited state) of L100R1&S226R1 recorded at 220 K, 235 K, and 245 K. The difference spectra show typical features of the M intermediate: D85 is protonated, revealed by a positive band at 1761 cm^{-1} and the Schiff base is deprotonated, indicated by the negative peak at 1186 cm^{-1}. Evidence for a small fraction of intermediate N is visible in the absorbance changes in the amide I region only at 245 K.

The distances between the nitroxide side chains were determined from the recorded EPR spectra according to the method of Steinhoff et al. (1997). This method provides exact values for the inter-spin distance and the distance distribution width in the distance range between 0.8 and 2.2 nm. Additional estimations of the inter-spin distances were made using the second moment EPR line-shape analysis (see Materials and Methods). Contributions of singly labeled proteins have only minor influence on the estimated distance values due to the r^{-6} dependence of the second moment. Furthermore, contributions of exchange interaction, which may be significant for inter-spin distances less than 1 nm, can be disregarded, because the second moment is sensitive only to dipolar interaction (Van Vleck, 1948). The EPR spectra of all samples for the BR initial state and for the M intermediate are shown in Fig. 3. The spectrum of the initial state of L100R1 and S226R1 shows significant broadening compared with the superposition of the spectra of the singly spin-labeled samples L100R1 plus S226R1. Fitting of simulated spectra to the spectra of the doubly spin-labeled L100R1&S226R1 agree quantitatively with the experimental data (not shown). The best fit yields an average inter-spin distance of 1.4 ± 0.1 nm and an amount of 50% non-interacting nitroxides (Table 1). This percentage results from singly spin-labeled proteins and is in agreement with the determined spin label to BR ratio of 140–160%. The second moment analysis yields an inter-spin distance of 1.5 ± 0.1 nm. Here, the non-interacting fraction of the nitroxides was neglected, resulting in a small (~5%) systematic deviation toward higher distance values.

The influence of the spin-spin interaction on the spectrum is considerably larger for the sample trapped in the M intermediate as revealed by the comparison of the normalized spectra. The mean value of the inter-spin distance determined by the spectral fitting procedure yields 1.2 ± 0.1 nm. Again, all other parameters were held fixed according to the values found for the BR initial state. The distance value estimated from the second moment of the spectra yields 1.3 ± 0.1 nm, which is again in agreement with the result from the fitting analysis. A different picture evolves for the doubly spin-labeled sample V101R1&A160R1 (Fig. 3 *b*). In particular, the BR initial-state spectrum shows broad lines due to spin-spin interaction, which are pronounced in the low- and high-field regions. The spectrum determined for the trapped M intermediate is virtually identical. Fitting of simulated powder spectra and the second moment calcu-

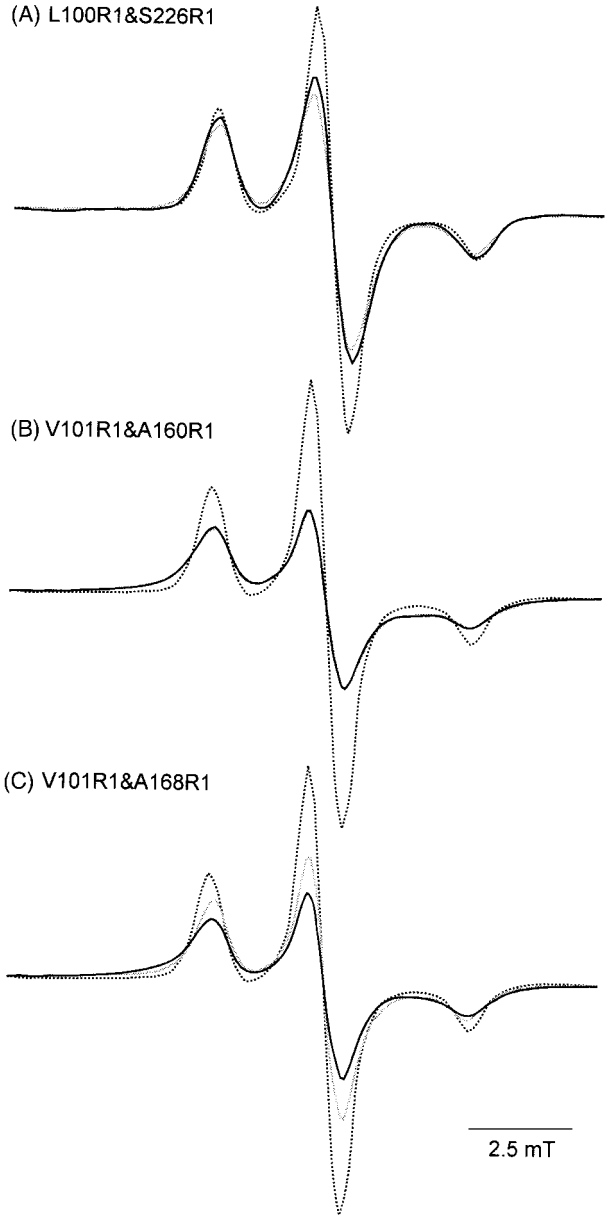

FIGURE 3 EPR spectra of doubly labeled BR recorded at 170 K. (*a*) Superposition of the first-derivative absorption spectra of the singly spin labeled mutants L100R1 and S226R1 (*dotted line*). The spectrum of the double mutant L100R1&S226R1 (*black line*) in the initial state shows line broadening due to the dipolar interaction between the spin label pairs. Illumination at 220 K and fast cooling to 170 K increases the line broadening for the doubly labeled mutant (*gray line*). (*b*) The spectrum of the double mutant V101R1&A160R1 (*black line*) shows pronounced dipolar broadening compared with the superposition of the spectra of the singly labeled mutants V101R1 and A160R1 (*dotted line*). Illumination at 220 K does not change the dipolar interaction for the doubly labeled mutant (*gray line*). (*c*) The spectrum of the double mutant V101R1&A168R1 (*black line*) in the initial state is dipolar broadened to a similar extent as revealed by the comparison with the superposition of the spectra of the singly labeled mutants (*dotted line*). Illumination at 220 K and fast cooling to 170 K decreases the line width for the doubly labeled mutant (*gray line*). All spectra are normalized to a constant spin number. The distances between the spin label pairs are given in Table 1.

lations confirm identical inter-spin distances for both states and yield distance values of 0.8 nm and 1.0 nm, respectively. A similar line shape evolves for V101&A168R1 in the BR initial state (Fig. 3 *c*). The line width is considerably reduced in the trapped M intermediate spectrum revealing a decreased spin-spin interaction. The inter-spin distances for the BR initial state and the M intermediate are calculated to be 0.7 and 0.8 nm, respectively. The second moment analysis of the BR initial state spectrum yields an inter-spin distance of 1.0 nm. For the M intermediate this value increases to 1.1 nm, confirming the 0.1-nm distance increase between the nitroxides at position 101 and 168 during the BR-to-M transition. The deviation from the results of the fitting is due to neglecting the fraction of singly spin-labeled proteins in the second moment analysis and its insensitivity against exchange interaction, which may bias the fitting results in the distance regime below 1 nm.

MD simulations of the doubly spin-labeled bacteriorhodopsin mutants L100R1&S226R1, V101R1&A160R1, and V101R1&A168R1 were performed to compare the EPR results with the x-ray data. From a MD trajectory of 6-ns length the distances trajectory between the nitroxide nitrogen atoms were extracted. The resulting distance distributions were fitted by a single Gaussian for L100R1&S226R1 and V101R1&A160R1 and by a superposition of two Gaussians for V101R1&A168R1. The mean distance between V101R1 and A160R1 amounts to 0.6 nm with a half width, σ, of 0.1 nm, the distance between L100R1 and S226R1 is 1.4 nm with $\sigma = 0.1$ nm (cf. Table 1). The distribution of the distance between V101R1 and A168R1 shows two extremes, the first at 0.8 nm with $\sigma = 0.1$ nm and the second at 1.0 nm with $\sigma = 0.2$ nm. Considering the lower limit of the distance determination via dipolar broadening due to effects of exchange interaction, the experimental results agree reasonably with the distance value determined by the MD simulations.

Inter-spin distances determined at room temperature

Room-temperature EPR spectra ($T = 293$ K) contain information about the secondary and tertiary structure of the nitroxide binding site and allow us to follow structural changes with a time resolution in the millisecond time range (Hubbell and Altenbach, 1994; Steinhoff et al., 1994; Rink et al., 2000). The spectra of L100R1, A160R1, and A168R1 consist of two spectral components (Fig. 4 and Fig. 2 of Pfeiffer et al., 1999). Spin label side chains being located close to a helix-helix contact interface were shown to exhibit this type of spectrum. The structural data locate A160R1 and A168R1 within the contact interface of helices E and F (Fig. 1), in agreement with the above finding. The immobilized component of L100R1 reflects a nitroxide position located in the entrance of the proton channel

TABLE 1 Inter-spin distances (in nm) of nitroxide pairs L100R1&S226R1, V101R1&A160R1, and V101R1&A168R1 in the BR initial state and in intermediate M

		L100R1&S226R1		V101R1&A160R1		V101R1&A168R1	
T/*K*	Method*	BR	M	BR	M	BR	M
293	$\langle \Delta B_D^2 \rangle$	1.3 ± 0.1	–	1.0 ± 0.1		1.1 ± 0.1	
170	$\langle \Delta B_D^2 \rangle$	1.5 ± 0.2	1.3 ± 0.1	1.0 ± 0.1	1.0 ± 0.1	0.9 ± 0.1	1.0 ± 0.1
170	Fit	1.4 ± 0.1	1.2 ± 0.1	0.8 ± 0.1	0.8 ± 0.1	0.7 ± 0.1	0.8 ± 0.1
	MD(NO-NO)	1.4 ± 0.1		0.6 ± 0.1		0.8 ± 0.1	
100	(C_α-C_α)	1.0		0.5		0.9	
93	EM(C_α-C_α)	1.1	0.8	0.5	0.5	0.8	1.0

*Inter-spin distances were determined from the second moment EPR line-shape analysis, $\langle \Delta B_D^2 \rangle$ or by means of spectral fitting (see Materials and Methods). The width of the distance distribution was restrained to 0.2 nm for all samples. MD simulations were performed on the basis of the x-ray data (Essen et al., 1998) with modeled spin labels. The electron microscopy (EM) data show the C_α-C_α distances for wild-type BR (BR) and for the triple mutant D96G, F171C, F219L (M) (Subramaniam et al., 2000).

most probably in contact with helix G or A. This is furthermore supported by the reduced polarity in the vicinity of the nitroxide as revealed by W-band EPR spectroscopy (Steinhoff et al., 2000). The mobile component may be due to a nitroxide side chain orientated toward the aqueous phase. The spectrum of V101R1 reflects intermediate immobilization, in agreement with former results where this mutant was analyzed in detail (Steinhoff et al., 1994; Rink et al., 2000). The spectrum of S226R1 corresponds to an immobilized nitroxide in agreement with the structural data showing this side-chain orientation toward helix F.

In addition to the modulation due to the nitroxide mobility the room temperature spectra of the doubly labeled mutants are influenced by spin-spin interaction. The dynamic dipolar interaction is not averaged for rotational correlation times of the inter-spin vector exceeding $2\hbar r^3/3\hbar g^2\beta^2$, where $\hbar$ is the Planck constant divided by 2π, g is the g factor, and β is the Bohr magneton. Thus, inter-spin distances less than 2 nm lead to considerable line broadening for correlation times exceeding 50 ns. The rotational correlation time of the inter-spin distance vector corresponds approximately to that of the whole protein, which in the case of BR in native purple membrane sheets is in the microsecond time range. Due to the residual motion of the nitroxides the inter-spin vector performs additional orientation fluctuations in the nanosecond time range. However, this fluctuation is strongly restricted in its angular amplitude. Hence, we conclude that an averaging of the dipolar interaction within the present BR samples can be neglected at room temperature.

For V101R1&A160R1 and V101R1&A168R1 the comparison with the superposition of the singly spin-labeled mutants reveals significant line broadening due to spin-spin interaction. The dipolar interaction between the two nitroxides is not that pronounced in the pair L100R1&S226R1, but it is still visible in the spectrum. Because exact spectral simulation is complicated due to the anisotropic nature of the nitroxide motion, the inter-spin distances were determined by means of the second moment analysis. This calculation yields inter-spin distance values of 1.0 nm for V101R1&A160R1, 1.1 nm for V101R1&A168R1, and 1.3

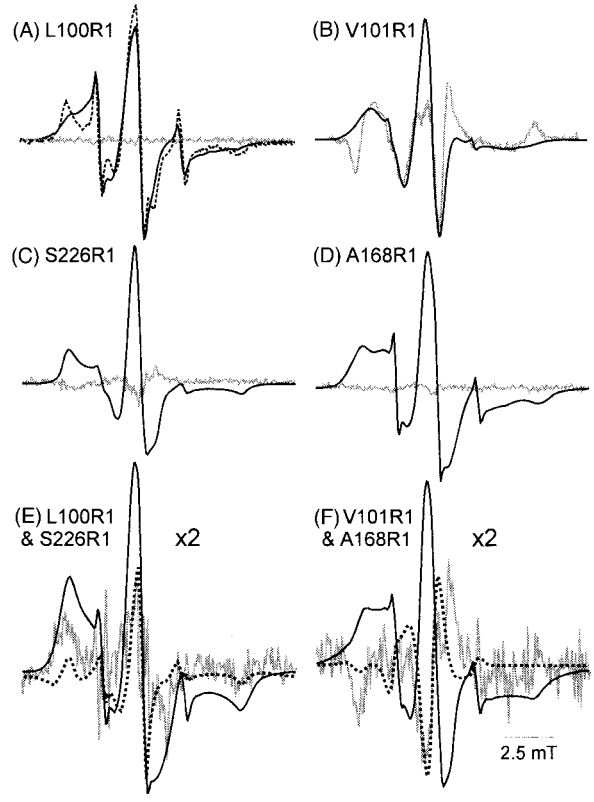

FIGURE 4 Steady-state EPR spectra (*black line*) and kinetic difference spectra (*gray line*) recorded at room temperature. (*a*) L100R1 prepared with DTT (*solid line*) and β-mercaptoethanol (*dashed line*) (see Materials and Methods); (*b*) V101R1; (*c*) S226R1; (*d*) A168R1; (*e*) L100R1&S226R1; (*f*) V101R1&A168R1. For both double mutants (*e* and *f*) a calculated difference spectrum based on changes in dipolar interaction is shown additionally (*dotted line*), in the case of *e* with the assumption of a transient decrease of the inter-spin distance and in the case of *f* with the assumption of a transient increase of the inter-spin distance. All spectra are normalized to a constant spin number. The amount of unbound spin label, which is responsible for the narrow lines in the spectra of L100R1, L100R1&S226R1, and V101R1&A168R1, is smaller than 2%, except for $^{\beta\text{-Me}}$L100R1 (~15%).

nm for L100R1&S226R1. These values agree reasonably well with the results determined from the frozen samples (see Table 1).

Kinetic difference spectra between the initial and the photo-excited states

After initiation of the photocycle with a light flash, the spectral difference between the initial state and the excited states were directly detected during a B-field scan (see Materials and Methods). The results are shown in Fig. 4. EPR spectral changes of doubly spin-labeled BR can originate from two sources. Alterations of the structure close to the spin label binding sites during the photocycle will result in changes of the motional restriction of the nitroxide and thus lead to different EPR spectra. Second, inter-spin distance changes during the photocycle entail changes of the spin-spin interaction and result in spectral changes. The differentiation between both effects is feasible only by comparison of the difference spectra of the singly spin-labeled mutants with that of the doubly spin-labeled sample. In addition, spectral simulations were performed to determine the spectral changes due to changes of the strength of the dipolar broadening. For this purpose the experimental spectrum of the doubly spin-labeled mutant was convoluted with a Gaussian to obtain a spectrum with increased dipolar interaction and subtracted from the unmodified experimental data (Fig. 4, *e* and *f*).

The kinetic difference spectra of L100R1 and A168R1 do not show any or only small mobility changes of the nitroxide side chain (Fig. 4, *a* and *d*) as already reported (Rink et al., 2000). In contrast, the difference spectrum of V101R1 shows that the nitroxide's side chain is transiently immobilized (Fig. 4 *b*) again in agreement with former results (Steinhoff et al., 1994). The difference spectrum of the double mutant V101R1&A168R1 differs significantly from that of the single mutant V101R1, showing that distance changes dominate the difference spectrum (Fig. 4 *f*). Its spectral shape is consistent with an increase of the inter-spin distance between V101R1 and A168R1 and an immobilization of V101R1.

The difference spectrum for S226R1 shows only small changes due to a transient mobilization of the nitroxide side chain (Fig. 4 *c*). Again, the difference spectrum of the double mutant L100R1&S226R1 reveals a completely different shape (Fig. 4 *e*). Comparison of this spectrum with a simulated difference spectrum that was calculated on the assumption of a transient inter-spin distance decrease shows qualitative agreement. The residual deviations are explainable due to the residual mobility change of S226R1, which additionally contribute to the experimental difference spectrum but is not accounted for in the calculated difference spectrum. Thus, the interpretation of the spectral changes of V101R1&A168R1 and L100R1&S226R1 observed during the photocycle at room temperature agrees with the results of the low-temperature measurements.

EPR spectral changes and absorbance changes in the visible spectrum

The photocycle kinetics is a useful measure for the integrity of BR; furthermore, the characterization of the photocycle is necessary for the interpretation of the EPR kinetics. EPR and optical absorbance changes were measured as described in Materials and Methods. The nomenclature of the time constants follows that of Hessling et al. (1993): τ_5 and τ_2 describe the disappearance of L and the appearance of M; τ_4 reflects the M-decay and the rise of N and O; τ_3 contributes to the decays of intermediates M, N, and O; and τ_6 is assigned to the decay of N to the BR initial state. In some cases, additional time constants, τ_8, and τ_9, which both describe the BR recovery, are necessary. The results are given in Table 2. For V101R1 and S226R1 and for the double mutants consideration of τ_3 did not further improve the fits so that this parameter was omitted. Compared with the wild type, the rates describing the rise (not shown) and the decay of M are not much altered by the exchange of the native amino acids by a spin-labeled cysteine. τ_6 is in-

TABLE 2 Time constants (in ms) of the rise and decay of the transients in the visible spectrum and of the EPR spectral changes

	τ_4	τ_6	τ_8	τ_9	$\tau_{EPR\text{-}1}$*	$\tau_{EPR\text{-}2}$	$\tau_{EPR\text{-}3}$
Wild type	2.2	18					
L100R1	0.8	100	390				
V101R1	8.2	180	820		7.8	185	530
A168R1	3.4	74					
S226R1	1.5	75	140	770	2.0	83	530
V101R1&A168R1	11.9	68	305		3.1	30	180
L100R1&S226R1	2.6	82	400	1950	3	158	1800

The time constants result from a multi-exponential fitting of the absorbance transients in the visible spectrum. The rates of L100R1 and A168R1 are taken from Pfeiffer et al. (1999) and Rink et al. (2000). L100R1, A160R1, and A168R1 show no EPR transient. The standard deviations of the time constants determined in the visible are less than 10%. The respective values determined from the EPR transients are less than 15%.

*To account for the rise time of the spectrometer, the rise time of the EPR spectral change was deconvoluted with the response function of the experimental setup (1 ms).

creased up to 10-fold, decreasing the recovery rate of the initial state for all mutants. This is particularly the case for S226R1 and for the double mutant L100R1&S226R1, where the two additional time constants, τ_8 and τ_9, contribute significantly to the initial state recovery.

The kinetics of the EPR signal change was resolved by detection of the amplitude changes at fixed B-field positions, where the EPR difference spectrum exhibit local extremes. For S226R1 and L100R1&S226R1 the time constants for the rise of the EPR transients are similar to the corresponding time constants of the decay of the M intermediate, τ_4 (Fig. 5 and Table 2). The at least bi-exponential decay of the EPR transients coincides with late initial state recovery determined by τ_8 and τ_9. The kinetics of the nitroxide at position 101 shows the transient immobilization that was described in detail by Steinhoff et al. (1994) and Rink et al. (2000). The EPR transient rises with the decay of the M intermediate and vanishes with the recovery of the initial state. For the double mutant V101R1&A168R1 the rise of the EPR transient is faster than the M-decay (Fig. 5 *a*). So the conformational change must be independent from the reprotonation of the Schiff base, for which the disappearance of the optical transient at 415 nm is indicative.

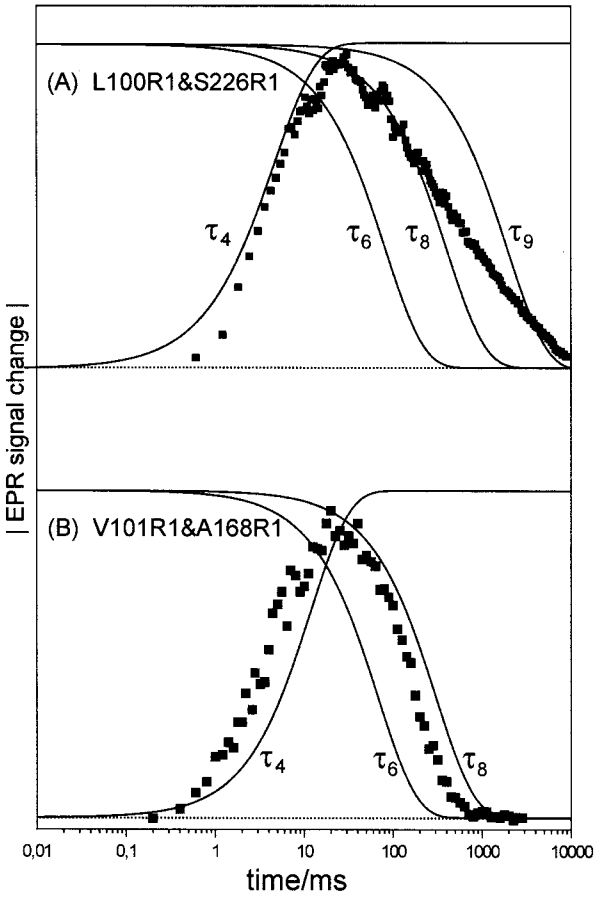

FIGURE 5 EPR signal changes after photo-excitation. The solid lines show the time course of the dominating rates determined by a multi-exponential fit of the visible spectra. The comparison of the EPR transient spectra with the absorbance changes allows an assignment of the conformational changes to the optically characterized intermediates. The time constants τ_4 are convoluted with the response function of the experimental setup to facilitate comparison of EPR and VIS data. Values of the time constants are given in Table 2.

DISCUSSION

One fundamental question under debate regarding the mechanism of proton transport in BR is the magnitude and the time course of the conformational change in M and N. The picture reported in the literature is diverse, and this is mostly attributed to the different methods of stabilization of the M intermediate. In general, the stabilized M contains more or less admixtures of the L and N intermediate. In addition, to overcome possible problems of crystal packing

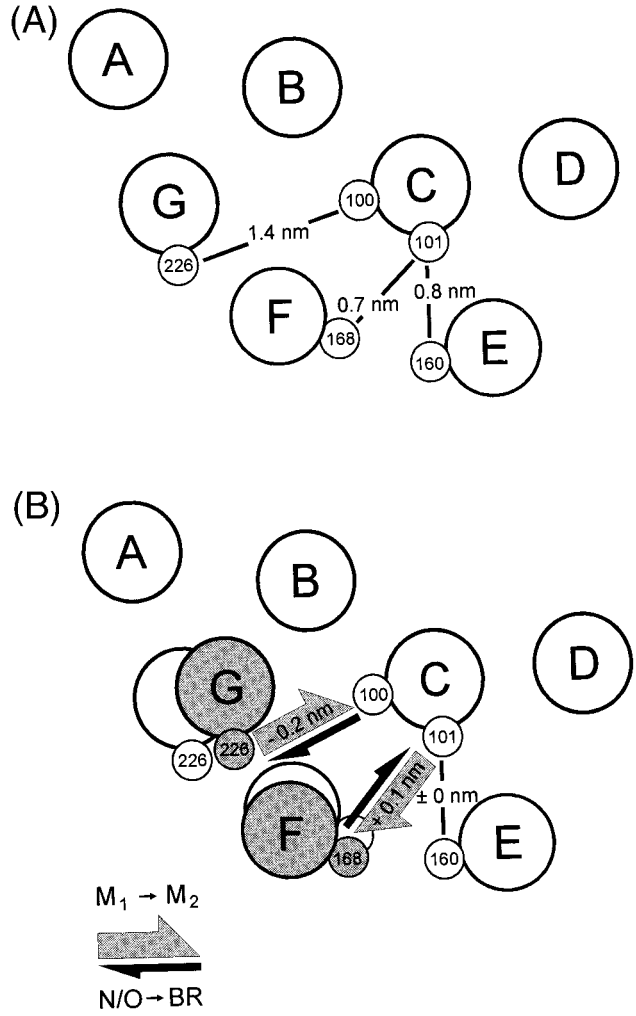

FIGURE 6 Schematic display of the top view of the cytoplasmic structure of BR. Inter-spin distances in the BR initial state (*a*) and distance changes during the photocycle (*b*) are shown. The low-temperature EPR data reveal an outward movement of helix F by 0.1 nm accompanied by an inward shift of the cytoplasmic terminus of helix G by 0.2 nm already visible in the late M intermediate (*gray*).

on the conformational dynamics we apply here the DSDSL approach and follow local structural changes in real time with millisecond time resolution under physiological conditions in the natural membrane.

Our results are summarized in Fig. 6. The inter-spin distance values in the BR ground state determined by EPR spectroscopy are in good agreement with the inter-nitroxide distance values determined from MD simulations on the basis of the x-ray data (Essen et al., 1998) (Table 1). The C_α-C_α distances determined from x-ray and electron diffraction correspond also well if we take the length of the spin-label side chain into account (~0.6 nm; cf. Fig. 6 *a* and Table 1). This shows that DSDSL is able to provide distances between spin labels with an accuracy of 0.1 nm.

The inter-spin distances in the BR initial state at room temperature and at 170 K agree within experimental errors of 0.1 nm, showing that no gross structural changes occur upon freezing the protein. The small deviations at V101R1&A168R1 between the room-temperature and low-temperature data may result from residual motional averaging effects of the dipolar interaction at 293 K. The second moment analysis is found to be a suitable supplement of the distance analysis by the fitting protocol, especially for inter-spin distances less than 1.2 nm and for immobilized non-frozen samples.

Conformational changes during the photocycle are determined by evaluation of the spin-spin interaction between the spin labels attached to the C-D loop (V101R1) and helix F (A168R1). They reveal an increase of the inter-spin distance in the trapped M intermediate compared with the BR initial state (Fig. 6 *b*) leading to an outward movement of helix F of 0.1 nm. No additional distance increase could be monitored for samples composed of a mixture of intermediates M and N. Hence, the maximum F helix shift is already present in intermediate M. The direction and magnitude of the F helix movement agrees with recent x-ray data (Sass et al., 2000) and with the electron crystallography data of the triple mutant D96G, F171C, F219L, in which the full extent of the light-driven conformational change is thought to be present with or without illumination (Subramaniam and Henderson, 2000). No distance change is detectable between positions 101 and 160, which are located at the cytoplasmic end of helix E. The resulting outward movement of helix F leads to an opening of the proton channel in agreement with the interpretation of earlier SDSL data (Rink et al., 2000).

Spin labels attached to the last cytoplasmic turn of helix C, the C-D loop, or the first turn of helix D show only mobility changes if they are oriented in the direction of the proton channel or the E-F loop. The consequent conclusion that the region of the C-D loop performs no large movements is in agreement with x-ray diffraction and electron crystallography data, which show only minor structural changes in this region (Subramaniam et al., 1999).

The decrease of the inter-spin distance between positions 100 and 226 by 0.2 nm in the trapped intermediate M strongly suggests a movement of helix G in the direction of the proton channel (cf. Fig. 6 *b*). This result is again in agreement with the structural differences between the BR wild type and the triple mutant (cf. Table 1) (Subramaniam and Henderson, 2000). A displacement of helix G of similar direction and extent was also concluded from x-ray diffraction studies of the mercury-labeled I222C (Oka et al., 1999), whereas the x-ray crystallography data of Sass et al. (2000) do not show significant distance changes between the C_α atoms of the respective residues for the BR initial state and intermediate M. The discrepancy within the results of the electron diffraction and x-ray methods may be a consequence of inhibited helix movements in the three-dimensional crystal. The displacements of helices G and F reported here transiently immobilize the nitroxide side chains at positions 166 and 170 in the helix-helix interface as was observed in our recent study (Rink et al., 2000). Furthermore, this observation rules out an additional anti-clockwise transient rotation of helix F, which was recently suggested by Xiao et al. (2000). For several positions analyzed by these authors the nitroxide side chains show large transient mobility changes during the photocycle (e.g., positions 167 and 171; see Rink et al., 2000). Thus, it seems that the inter-spin distances given by Xiao et al. (2000) are biased by a repacking of the nitroxide side chains.

How are the movements of the helices F and G related to the photocycle reactions? The F-helix displacement (V101R1&A168R1) at 293 K is considerably faster than the M-to-N transition (see Table 1 (compare τ_4 and $\tau_{EPR\text{-}1}$) and Fig. 5). In addition, the conformational change is already present in the low-temperature M intermediate as shown by the EPR and FT-IR data of the trapped intermediate. The G-helix movement (L100R1&S226R1) occurs in phase with the M-to-N transition. However, the low-temperature data show the G-helix shift being present already in the trapped M state concomitant with the displacement of helix F. This apparent discrepancy between the low- and the room-temperature data can be resolved by assuming different activation enthalpies for the reprotonation reaction of the Schiff base in the M-to-N transition and for the conformational change in the M_1-to-M_2 transition. The deviation in the rise time of the EPR transients ($\tau_{EPR\text{-}1}$) compared with the optically determined M-to-N transition may then be a consequence of a modulation of the rates of the M_1-to-M_2-to-N transitions by temperature and/or mutation. In the case that the conformational alterations occur during the M_1-to-M_2 transition and are retained in intermediate N, the rise time of the transient EPR signal coincides with that of the M_1-to-M_2 transition. If a shorter decay than rise time of intermediate M_2 prevents M_2 from accumulation, the structural change occurs with a time constant identical to that of the optically observed M-to-N transition. This may be the case for the movement of helix G at room temperature. Due to the

different mutations for spin labeling at the helices F and G they may slightly differ in their time course at room temperature. However, lowering the temperatures may increase the decay time of intermediate M_2 more than the rise time. This would allow accumulation of intermediate M_2 at low temperatures, and the conformational change would be visible already in the late M state in agreement with our data.

Time-resolved FT-IR double-flash experiments indicate a movement around the Y185/P186 peptide bond during the M_1-to-M_2 transition by which the Schiff base is oriented from the proton release to the proton uptake side (Hessling et al., 1993). Such hinge torsion at Y185/P186 results in the movement of the cytoplasmic end of helix F resolved here by EPR spectroscopy (Fig. 6 *b*). We conclude that this movement is involved in the reset mechanism of the pump by facilitating reprotonation of the Schiff base, e.g., by allowing an entrance of water molecules into the channel region. The resulting opening of the proton channel initiates the change of the pKa of D96, and a proton is transferred to the Schiff base during the succeeding M_2-to-N transition. However, the increase of the amide difference band at 1670/1660 cm^{-1} occurring during the M-to-N transition indicates a backbone structural movement that does not reflect the conformational change of the cytoplasmic moieties of helices F and G. The amide difference band increase does not correlate with the observed inter-spin distance changes. This is in agreement with the observation that amide band changes do not correlate with changes of helix F detected in x-ray diffraction experiments (Sass et al., 1997). Which peptide bond changes are reflected by the difference band at 1670/1660 cm^{-1} remains to be elucidated.

This paper shows that DSDSL provides intramolecular distances in the range of 1.0 to ~2.0 nm with an accuracy of 0.1 nm and allows us to follow structural changes at room temperature in real time with a resolution of milliseconds. The EPR dipolar interaction analysis method thus opens a wide field in the study of the structure and dynamics of proteins without crystallization under physiological conditions.

We thank R. Rammelsberg and A. Martin for their support concerning the optical and FT-IR measurements and C. Beier for MD simulations.

This work was supported by the Deutsche Forschungsgemeinschaft (SFB 394, C1, C2, and C8).

REFERENCES

Abragam, A. 1961. Principles of Nuclear Magnetism. Oxford University Press, Oxford, UK.

Dencher, N. A., D. Dresselhaus, G. Zaccai, and G. Büldt. 1989. Structural changes in bacteriorhodopsin during proton translocation revealed by neutron diffraction. *Proc. Natl. Acad. Sci. U.S.A.* 86:7876–7879.

Druckmann, S., N. Friedmann, J. K. Lanyi, R. Needleman, M. Ottolenghi, and M. Shewes. 1992. The back photoreaction of the M intermediate in the photocycle of bacteriorhodopsin: mechanism and evidence for two M species. *Photochem. Photobiol.* 56:1041–1047.

Essen, L. O., R. Siegert, W. D. Lehmannn, and D. Oesterhelt. 1998. Lipid patches in membrane protein oligomers: crystal structure of the bacteriorhodopsin-lipid complex. *Proc. Natl. Acad. Sci. U.S.A.* 95: 11673–11678.

Farrens, D. L., C. Altenbach, K. Yang, W. L. Hubbell, and H. G. Khorana. 1996. Requirement of rigid-body motion of transmembrane helices for light activation of rhodopsin. *Science.* 274:768–770.

Feix, J. B., and C. S. Klug. 1998. Site-directed spin labeling of membrane proteins and peptide-membrane interactions. *In* Spin Labeling: The Next Millenium. L. J. Berliner, editor. Plenum Press, New York. 251–281.

Ferrando, E., U. Schweiger, and D. Oesterhelt. 1993. Homologous bacterio-opsin-encoding gene expression via site-specific vector integration. *Gene.* 125:41–47.

Haupts, U., J. Tittor, and D. Oesterhelt. 1999. Closing in on bacteriorhodopsin: progress in understanding the molecule. *Annu. Rev. Biophys. Biomol. Struct.* 28:367–399.

Hessling, B., J. Herbst, R. Rammelsberg, and K. Gerwert. 1997. Fourier transform infrared double-flash experiments resolve bacteriorhodopsins M-1 to M-2 transition. *Biophys. J.* 73:2071–2080.

Hessling, B., G. Souvignier, and K. Gerwert. 1993. A model-independent approach to assigning bacteriorhodopsin's intramolecular reactions to photocycle intermediates. *Biophys. J.* 65:1929–1941.

Hubbell, W. L., and C. Altenbach. 1994. Investigation of structure and dynamics in membrane proteins using site-directed spin labeling. *Curr. Opin. Struct. Biol.* 4:566–573.

Hubbell, W. L., D. S. Cafiso, and C. Altenbach. 2000. Identifying conformational changes with site-directed spin labeling. *Nat. Struct. Biol.* 7:735–739.

Hubbell, W. L., A. Gross, R. Langen, and M. A. Lietzow. 1998. Recent advances in site-directed spin labeling of proteins. *Curr. Opin. Struct. Biol.* 8:649–656.

Hubbell, W. L., H. S. McHaourab, C. Altenbach, and M. A. Lietzow. 1996. Watching proteins move using site-directed spin labeling. *Structure.* 4:779–783.

Hustedt, E. J., and A. H. Beth. 1999. Nitroxide spin-spin interactions: applications to protein structure and dynamics. *Annu. Rev. Biophys. Biomol. Struct.* 28:129–153.

Kamikubo, H., M. Kataoka, G. Varo, T. Oka, F. Tokunaga, R. Needleman, and J. Lanyi. 1996. Structure of the N intermediate of bacteriorhodopsin revealed by x-ray diffraction. *Proc. Natl. Acad. Sci. U.S.A.* 93: 1368–1390.

Kensch, O., B. A. Connolly, H. J. Steinhoff, A. McGregor, R. S. Goody, and T. Restle. 2000. HIV-1 reverse transcriptase-pseudoknot RNA aptamer interaction has a binding affinity in the low picomolar range coupled with high specificity. *J. Biol. Chem.* 275:18271–18278.

Krebs, M. P., T. Hauss, M. P. Heyn, U. L. RajBhandary, and H. G. Khorana. 1991. Expression of the bacterioopsin gene in *Halobacterium halobium* using a multicopy plasmid. *Proc. Natl. Acad. Sci. U.S.A.* 88:859–863.

Lamoureux, G. V., and G. M. Whitesides. 1993. Synthesis of dithiols as reducing agents for disulfides in neutral aqueous solution and comparison of reduction potential. *J. Org. Chem.* 58:633–641.

Lanyi, J. K. 1998. The local-access mechanism of proton transport by bacteriorhodopsin. *Biochim. Biophys. Acta. Bioenerg.* 1365:17–22.

Likhtenstein, G. I. 1976. Spin Labeling Methods in Molecular Biology. John Wiley, New York.

Luecke, H., B. Schobert, H.-T. Richter, J.-P. Cartailler, and J. K. Lanyi. 1999. Structural changes in bacteriorhodopsin during ion transport at 2 angstrom resolution. *Science.* 286:255–260.

Mchaourab, H. S., K. J. Oh, C. J. Fang, and W. L. Hubbell. 1997. Conformation of T4 lysozyme in solution. Hinge-bending motion and the substrate-induced conformational transition studied by site-directed spin labeling. *Biochemistry.* 36:307–316.

Mollaaghababa, R., H. J. Steinhoff, W. L. Hubbell, and H. G. Khorana. 2000. Time-resolved site-directed spin-labeling studies of

bacteriorhodopsin: loop-specific conformational changes in M. *Biochemistry.* 39:1120–1127.

Oesterhelt, D., and W. Stoeckenius. 1974. Isolation of the cell membrane of *Halobacterium halobium* and its fractionation into red and purple membrane. *Methods Enzymol.* 31:667–678.

Oka, T., H. Kamikubo, F. Tokunaga, J. K. Lanyi, R. Needleman, and M. Kataoka. 1999. Conformational change of helix G in the bacteriorhodopsin photocycle: investigation with heavy atom labeling and x-ray diffraction. *Biophys. J.* 76:1028–1023.

Perozo, E., D. M. Cortes, and L. G. Cuello. 1999. Structural rearrangement underlying K^+-channel activation gating. *Science.* 285:73–78.

Pfeiffer, M., T. Rink, K. Gerwert, D. Oesterhelt, and H. J. Steinhoff. 1999. Site-directed spin-labeling reveals the orientation of the amino acid side-chains in the E-F loop of bacteriorhodopsin. *J. Mol. Biol.* 287: 163–171.

Rammelsberg, R., B. Hessling, H. Chorongiewski, and K. Gerwert. 1997. Molecular reaction mechanisms of proteins monitored by nanosecond step-scan FT-IR difference spectroscopy. *Appl. Spectrosc.* 51:558–562.

Rammelsberg, R., G. Huhn, M. Lübben, and K. Gerwert. 1998. Bacteriorhodopsins intramolecular proton-release pathway consists of a hydrogen-bonded network. *Biochemistry.* 37:5001–5009.

Rink, T., M. Pfeiffer, D. Oesterhelt, K. Gerwert, and H. J. Steinhoff. 2000. Unraveling photoexcited conformational changes of bacteriorhodopsin by time resolved electron paramagnetic resonance spectroscopy. *Biophys. J.* 78:1519–1530.

Sass, H. J., G. Bueldt, R. Gessenich, D. Hehn, D. Neff, R. Schlesinger, J. Berendzen, and P. Ormos. 2000. Structural alterations for proton translocation in the M state of wild-type bacteriorhodopsin. *Nature.* 406: 649–652.

Sass, H. J., I. W. Schachowa, G. Rapp, M. H. Koch, D. Oesterhelt, N. A. Dencher, and G. Buldt. 1997. The tertiary structural changes in bacteriorhodopsin occur between M states: x-ray diffraction and Fourier transform infrared spectroscopy. *EMBO J.* 16:1484–1491.

Steinhoff, H. J., R. Mollaaghababa, C. Altenbach, K. Hideg, M. Krebs, H. G. Khorana, and W. L. Hubbell. 1994. Time-resolved detection of structural changes during the photocycle of spin-labeled bacteriorhodopsin. *Science.* 266:105–107.

Steinhoff, H. J., N. Radzwill, W. Thevis, V. Lenz, D. Brandenburg, A. Antson, G. Dodson, and A. Wollmer. 1997. Determination of interspin distances between spin labels attached to insulin: comparison of electron paramagnetic resonance data with the x-ray structure. *Biophys. J.* 73: 3287–3298.

Steinhoff, H. J., A. Savitsky, C. Wegener, M. Pfeiffer, M. Plato, and K. Möbius. 2000. High-field EPR studies of the structure and conformational changes of site-directed spin labeled bacteriorhodopsin. *Biochim. Biophys. Acta*. 1457:253–262.

Subramaniam, S., M. Gerstein, D. Oesterhelt, and R. Henderson. 1993. Electron diffraction analysis of structural changes in the photocycle of bacteriorhodopsin. *EMBO J.* 12:1–8.

Subramaniam, S., and R. Henderson. 2000. Molecular mechanism of vectorial proton translocation by bacteriorhodopsin. *Nature.* 406: 653–657.

Subramaniam, S., I. Lindahl, P. Bullough, A. R. Faruqi, J. Tittor, D. Oesterhelt, L. Brown, J. Lanyi, and R. Henderson. 1999. Protein conformational changes in the bacteriorhodopsin photocycle. *J. Mol. Biol.* 287:145–161.

Thorgeirsson, T. E., W. Z. Xiao, L. S. Brown, R. Needleman, J. K. Lanyi, and Y. K. Shin. 1997. Transient channel-opening in bacteriorhodopsin—an EPR study. *J. Mol. Biol.* 273:951–957.

Tiebel, B., N. Radzwill, L. M. Aung-Hilbrich, V. Helbl, H. J. Steinhoff, and W. Hillen. 1999. Domain motions accompanying Tet repressor induction defined by changes of interspin distances at selectively labeled sites. *J. Mol. Biol.* 290:229–240.

Van Vleck, J. H. 1948. The dipolar broadening of magnetic resonance lines in crystals. *Phys. Rev.* 74:1168–1183.

Váró, G., and J. K. Lanyi. 1991. Kinetic and spectroscopic evidence for an irreversible step between deprotonation and reprotonation of the Schiff base in the bacteriorhodopsin photocycle. *Biochemistry.* 30:5008–5015.

Vonck, J. 1996. A three-dimensional difference map of the N intermediate in the bacteriorhodopsin photocycle: part of the helix F tilts in the M to N transition. *Biochemistry.* 35:5870–5878.

Vonck, J. 2000. Structure of the bacteriorhodopsin mutant F219L N intermediate revealed by electron crystallography. *EMBO J.* 19:2152–2160.

Xiao, W., L. S. Brown, R. Needleman, J. K. Lanyi, and Y.-K. Shin. 2000. Light-induced rotation of a transmembrane alpha-helix in bacteriorhodopsin. *J. Mol. Biol.* 304:715–721.

Zimanyi, L., G. Varo, M. Chang, B. Ni, R. Needleman, and J. K. Lanyi. 1992. Pathways of proton release in the bacteriorhodopsin photocycle. *Biochemistry.* 31:8535–43.